# Estimator Based Amplitude Demodulation in High Speed Dynamic Atomic Force Microscopy

Andreas Schuh[1, a)] and Ivo W. Rangelow[1]

*Ilmenau University of Technology, Faculty of Electrical Engineering and Information Technology, Dept. of Microelectronic and Nanoelectronic Systems, Gustav-Kirchhoff-Str. 1, 98684 Ilmenau, Germany*

(Dated: October 26, 2014)

The amplitude demodulation in intermittent mode atomic force microscopy is one of the key elements in the z axis feedback loop. In combination with a controller it is used to keep an average distance of the cantilever to the sample and to form different signals for surface mapping. The demodulator's time constant and noise rejection is crucial for both image quality and imaging rate. Commonly, Lock-in amplifiers are used for this task. Alternative techniques proved to be faster but some with decreased robustness. Such methods include a demodulation based on the detection of each cycle's minimum and maximum. In this work, an alternative demodulation technique is presented. It is based on a combination of the minimum-maximum approach with an existing estimator based compensator. The estimator provides a noise reduced and decoupled sensor signal for each modeled eigenmode. Excited unmodeled eigenmodes and harmonics are filtered out that otherwise can distort a regular minimum-maximum method. As a result, dynamic modification and demodulation can be achieved simultaneously. In combination with the compensator the demodulation is a simple extension with little added complexity, compared to a compensator/Lock-in based setup. The demodulation methodology is validated by time domain signals and imaging of a calibration sample in the intermittent mode in air. In our study, an active cantilever with integrated actuation and sensing has been utilized.

[a)]andreas.schuh@tu-ilmenau.de

# I. INTRODUCTION

The invention of the Atomic Force Microscope (AFM)[1] has made the nanoscale investigation of a large variety of samples in different environments possible. The contact mode was utilized first, mainly for measuring the topography of a sample. High forces producing strong friction led to the development of dynamic modes such as the intermittent and non-contact mode. In the dynamic modes the demodulation of the amplitude, phase and frequency became a necessity for forming control signals and images. As a result, the feedback loop is extended by a demodulator, most often a Lock-in amplifier[2]. Other less popular methods are based on RMS/DC converters.

The Lock-in amplifier is a powerful tool to retrieve signals covered in noise. However, the demodulator is also an additional component in the feedback loop that further decreases the imaging bandwidth. Its filter time constant plays a crucial role in the two opposing measures feedback bandwidth and rejection of sensor noise. High feedback bandwidths require low filter time constants, whereas a good noise rejection needs higher constants. Usually, a trade-off between the two has to be found depending on the application and noise characteristic of the sensors. The cantilever sensor signal is recovered in respect to a reference signal. The reference signal is often similar to the signal used for the cantilever actuation. Consecutive filtering and additional operations result in the estimated amplitude. Figure 1 is a block diagram of its functionality indicating the different steps involved.

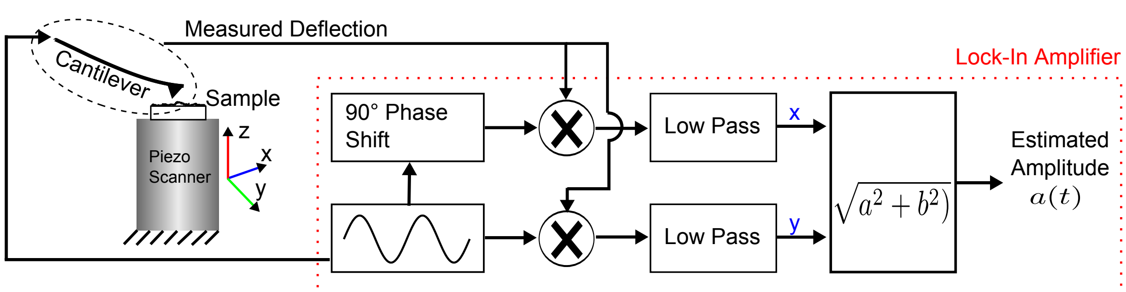


Figure 1: Principle of a regular Lock-in amplifier connected to a cantilever and delivering the estimated amplitude.

To increase the imaging bandwidth, Ando *et al.* have introduced an alternative approach based on peak holding[3]. The minimum and maximum peaks of each cycle of the cantilever's vibration signal are determined by an analog circuit. The resulting amplitude is then used instead of a Lock-in amplifier. A different detector is introduced by Blais and Rioux[4] and works with an FIR filter in discrete time. Fourier based methods have been developed by Kokavecz *et al.* that calculate the Fourier coefficients[5]. An improved method also conform with multifrequency AFM techniques is introduced by Karvinen and Moheimani[6], based on phase cancellation. Their publication also delivers an excellent overview of other existing methods.

One of the potential problems of a simple minimum-maximum demodulator is noise and signals of different frequencies superimposed on the sensor signal. This also prevents the operation in multifrequency AFM methods[7]. For example, excited higher harmonics appear in the cantilever during imaging in the intermittent mode. Such detected signal is indicated in Figure 2. The gray and black curves are the raw sensor signal and its noise filtered counterpart, respectively. Without proper precaution, such as bandpass filtering, these superimposed signals have an impact on the reliability of the detected amplitude.

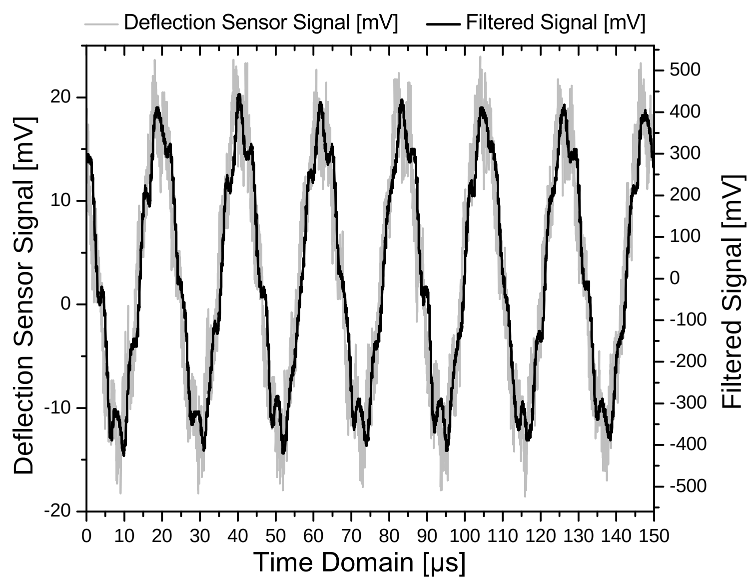


Figure 2: Higher harmonics excited while scanning a sample in the intermittent mode. The pronounced higher frequency is the $6^{\mathrm{th}}$ harmonic superimposed on the first resonance.

In this work, an estimator based compensator is extended by a simple amplitude demodulator. The compensator has been developed in our previous work. It is used to modify the dynamics of the cantilever probe in one or more eigenmodes. The dynamic modifications can be both in Q factor and resonance frequency of each modeled eigenmode. The estimated output of the compensator represents a filtered copy of the cantilever sensor deflection signal. The numerical difference of the two signals is used to correct the model uncertainties. In the following, the estimated sensor signal is used to connect the amplitude demodulators, one for each modeled eigenmode. The approach is also conform with multifrequency AFM techniques, such as bimodal AFM[8,9]. The methodology is based on finding the minimum and maximum of the estimated sensor deflection signal. It can simply be operated in addition to the control functionality of the compensator. The demodulator can be used by switching the AFM controller into contact mode and connecting the demodulated signals. In combination with the compensator the demodulator extension is of less complexity than adding a regular Lock-in amplifier to the compensator extended AFM setup. Also, the estimator incorporates similar dynamics as the cantilever. Following, the time constant of the demodulators are always matched with the time constants of the cantilever eigenmodes. The utilized cantilevers are active, meaning they incorporate actuation and deflection sensing into the beam[10,11].

The presented paper is organized as follows. Section II introduces the active cantilever technology used in this work to validate the demodulation methodology. In Section III, the amplitude detector based on an estimator and the minimum-maximum method is presented. The implementation into a Field Programmable Gate Array (FPGA) based system is outlined in Section IV. Section V presents the validation in the time domain and by scanning a sample in intermittent mode in air with a modified AFM setup. A conclusion is given in Section VI.

## II. COMPACT PIEZORESISITVE AND SELF-ACTUATED CANTILEVERS

The active cantilevers are equipped with integrated and highly sensitive 2-Dimensional Electron Gas (2DEG) piezoresistive sensors used as deflection read-out. In addition, they incorporate bimorph actuators and sharp tips[10,11]. The power dissipation of an applied current forces the layers with dissimilar heat coefficients to expand differently. Based on the layers' organization the cantilever bends vertically. An applied AC current coinciding with the mechanical resonance of the cantilever results in its transverse vibrations. The power dissipation is maximized by considering still acceptable drift in the measurements.

The 2DEG piezoresistive sensors are formed in the area of maximum vibrational sress, which is close to the cantilever base. By organizing the sensors in a Wheatstone bridge formation a significant improvement in the deflection sensitivity is achieved[12]. As the piezoresistive effect depends on the temperature[13], the resulting fluctuations on the cantilever sensor signal are of special concern. Two measures can be used to counteract this behavior. First, a temperature drift compensation has been introduced[12]. Second, piezoresistivity is significantly larger for low dopant concentrations. However, a high concentration can be used to achieve a low temperature dependence[14]. Also, the sensors are electrically isolated from the actuator and designed for minimum capacitive and thermal crosstalk.

The cantilever's thermo-mechanical noise floor is measured at $80\,\mathrm{fm}/\sqrt{Hz}$. In its fabrication, advantages are gained from recent high performance cantilever bulk fabrication technologies[10,15]. After formation of the tip by reactive ion etching the electrical shielding to prevent crosstalk is implanted. The piezoresistors are defined by a standard CMOS doping procedure, followed by a thermal annealing step. Then, a low stress silicon nitride layer is formed by PECVD for electrical passivation. The meander shaped metal actuator is placed on top of the passivation layer. The contact pads are realized thereafter. The cantilever thickness is defined by a backside anisotropic etching step. Finally, the cantilever's lateral dimensions are defined by a gas chopping etch process[16,17]. The fabrication is outlined in more detail in[11,18].

Figure 3 shows a typical active cantilever (SEM image). It is connected to electronic components required for actuation and sensor post-processing. The *Direct Digital Synthesis (DDS)* excites the cantilever at its resonances. The *Bridge Supply* is a static voltage resulting in a deflection signal at the inputs of the differential amplifier $G$. After amplification, the signal is processed through other components, such as the demodulator.

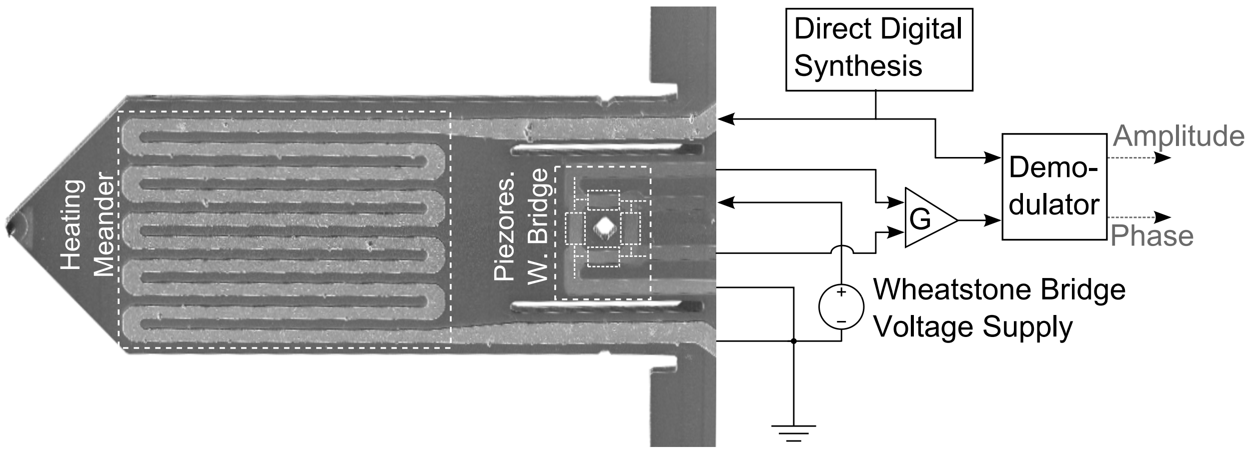


Figure 3: Active cantilever (SEM image) and its connections to electronic components for actuation and sensor post-processing.

## III. AMPLITUDE DEMODULATOR DESIGN

The amplitude demodulator is formed as an extension to the existing compensator (Figure 4). With its model, the estimator simulates the cantilever dynamics and is corrected via a feedback of gain $\mathbf{L}$. The estimated deflection output $\hat{y}$ ideally matches the sensed cantilever deflection signal $y$. Depending on $\mathbf{L}$, $\hat{y}$ is much reduced in noise. As a result, the decoupled $\hat{y}_i$ of the modeled eigenmodes $i$ are used for the amplitude demodulation instead of $y$, each with its own demodulator $D_i$.

### A. Compensator

The compensator with its estimator allows estimation of unmeasured states and the modification of the cantilever dynamics. The unmeasured signals are the velocity of the cantilever vibrations that are needed for affecting the Q factor. A discrete model of the cantilever with states $\mathbf{q}_k$, input $u_k$ and output $y_k$ can be represented as

$$\mathbf{q_{k+1}} = \bar{\mathbf{A}}\mathbf{q_k} + \bar{\mathbf{B}}u_k + w_k, \tag{1}$$

$$y_k = \bar{\mathbf{C}}\mathbf{q}_k + v_k, \tag{2}$$

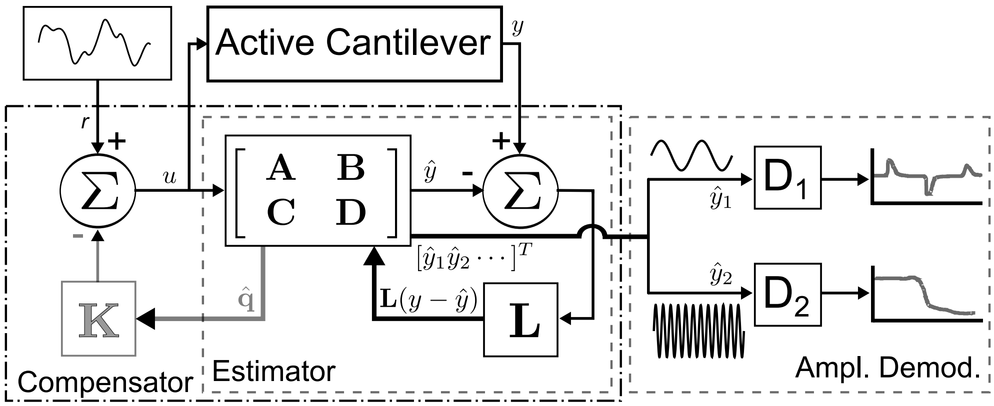


Figure 4: The overall amplitude demodulator attached to the compensator. Each $\hat{y}_i$ is fed to its own demodulator $D_i$.

where $\bar{\mathbf{A}}$, $\bar{\mathbf{B}}$ and $\bar{\mathbf{C}}$ are the experimentally determined matrices/vectors of the cantilever's state transition matrix $\mathbf{A}$, input vector $\mathbf{B}$ and output vector $\mathbf{C}$, respectively. The discrete time step is indicated by $k$. $w_k$ and $v_k$ are the cantilever and sensor measurement noise, respectively.

The model is formed by estimating the unknown coefficients. It is based on measured vibrational characteristics using an automatic system identification approach. The model can be represented in the modal form as

$$\bar{\mathbf{A}} = \begin{bmatrix} \bar{\mathbf{A}}_\mathbf{1} & \mathbf{0} & \cdots \\ \mathbf{0} & \bar{\mathbf{A}}_\mathbf{2} & \\ \vdots & & \ddots \end{bmatrix}, \bar{\mathbf{B}} = \begin{bmatrix} \bar{\mathbf{B}}_\mathbf{1} \\ \bar{\mathbf{B}}_\mathbf{2} \\ \vdots \end{bmatrix}, \bar{\mathbf{C}} = \begin{bmatrix} \bar{\mathbf{C}}_\mathbf{1} \\ \bar{\mathbf{C}}_\mathbf{2} \\ \vdots \end{bmatrix}^T. \tag{3}$$

In this balanced representation each eigenmode $i$ occupies an individual sub-matrix/sub-vector. The separation is beneficial for the amplitude detector described in Subsection III.B and the hardware implementation in Section IV. Following, a prediction estimator with the estimated states $\hat{\mathbf{q}}_k$ combined with a controller $\mathbf{K}$ can be formed to

$$\hat{\mathbf{q}}_\mathbf{k} = (\bar{\mathbf{A}} - \bar{\mathbf{B}}\mathbf{K} - \mathbf{L}\bar{\mathbf{C}})\hat{\mathbf{q}}_\mathbf{k-1} + \bar{\mathbf{B}}r_{k-1} + \mathbf{L}y_{k-1}, \tag{4}$$

where the feedback loop has been closed by $u_k = r_k - \mathbf{K}\hat{\mathbf{q}}_k$. $r_k$ and $u_k$ are the AFM controller generated actuation signal and the now modified cantilever input signal, respectively. The estimated deflection signal is

$$\hat{y}_k = \bar{\mathbf{C}}\hat{\mathbf{q}}_k. \tag{5}$$

Equations (4) and (5) form the compensator in Figure 4.

### B. Demodulator Extension

The compensator's $\hat{y}_k = \bar{\mathbf{C}}\hat{\mathbf{q}}_k$ is used to demodulate the amplitude. The demodulator is designed as an extension to the existing compensator (Figure 4) and, hence, can be operated in parallel to its control functionality.

The computation of $\hat{y}_k$ is reorganized if a multi-eigenmode compensator acting on two or more resonances is used. Then, the vector $\hat{y}_k$ is separated into each eigenmode's $\hat{y}_{k,i}$, which is simple in the model's modal form. $\hat{y}_k$ is then formed by summing all $\hat{y}_{k,i}$:

$$\begin{bmatrix} \hat{y}_{k,1} \\ \hat{y}_{k,2} \\ \vdots \end{bmatrix} = \begin{bmatrix} \bar{\mathbf{C}}_\mathbf{1} & 0 & \cdots \\ 0 & \bar{\mathbf{C}}_\mathbf{2} & \\ \vdots & & \ddots \end{bmatrix} \begin{bmatrix} \hat{\mathbf{q}}_{\mathbf{k,1}} \\ \hat{\mathbf{q}}_{\mathbf{k,2}} \\ \vdots \end{bmatrix} \Rightarrow \hat{y}_k = \hat{y}_{k,1} + \hat{y}_{k,2} + \cdots \tag{6}$$

Each $\hat{y}_{k,i}$ is connected to its own demodulator $D_i$, as indicated in Figure 4. This approach does not add any computational effort to the compensator itself, since computing $\hat{y}_{k,i}$ are intermediate steps towards the overall $\hat{y}_k$. As each $\hat{y}_{k,i}$ only represents the signal at a particular frequency, other eigenmodes and excited harmonics are filtered and not present. This strongly enhances the reliability of the attached demodulators.

As indicated earlier, the $D_i$'s are based on the minimum-maximum methodology. The work principle of each $D_i$ is schematically introduced in Figure 5. The dash-dotted curve is the estimated $\hat{y}_{k,i}$. Two levels *H-T* and *L-T* are set, giving a High and Low Threshold, respectively. It prevents the undesired activation of a new cycle near the '0' line due to noise. Hence, $\hat{y}_{k,i}$ needs to pass through both '0' and *H-T*/*L-T* before the consecutive cycle is activated. This is analog to the principle of a Schmitt trigger with its hysteresis. This behavior is also indicated by the dashed arrows in Figure 5. Then, the respective positive *Temp-Max* or negative *Temp-Min* detectors are activated, starting at value '0'. In each cycle, it stores the current sample if it is larger (positive part) or smaller (negative part) than its predecessor. After the following cycle is started (*L-T* or *H-T*) the respective previous value in *Temp-Max* or *Temp-Min* is stored as a new *Max* or *Min* value. Subtraction of *Min* from *Max* gives the demodulated peak-to-peak amplitude, which is updated every half-period of the vibration signal. It results in intermediate steps in the demodulated amplitude and an update time of twice the corresponding frequency. Following, a change in the amplitude requires up to a full signal period to be correctly detected.

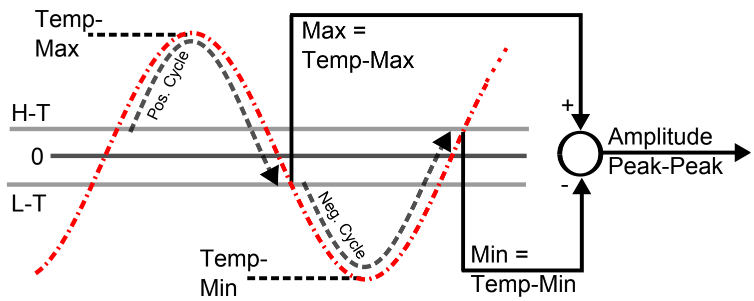


Figure 5: Functionality of the amplitude demodulator on a sinusoid $\hat{y}_{k,i}$ cantilever signal.

In this work, only the amplitude demodulation has been realized. However, the phase information can be easily added in a similar fashion. This is achieved by first obtaining a time stamp at a particular point in time of both the actuation and sensor signal. For example, when the signals are either crossing $H$-$T$ or $L$-$T$. The time difference of both time stamps in respect to a full period of the vibration frequency gives a phase between 0 and close to 1. The resolution is based on the demodulators internal clock frequency $f_d$. Hence, the maximum numerical phase would be $1 - 1/f_d$. A phase of 1 represents a full period and is equal to a phase of 0. Proper scaling can be used to adapt the phase to familiar values of 0 to 360.

## IV. IMPLEMENTATION

The demodulators combined with the compensator are implemented into an FPGA by using VHDL. The nano analytik GmbH SPM platform[19] offers 100 MHz ADC and DAC converters. A block diagram of the implementation is shown in Figure 6. The *Fast Loop* has a clock rate 100 MHz that samples at 100 MSa/s. After the AD-conversion in the *Fast Loop*, the samples are converted into single precision floating point and pushed into single sample buffers. The compensator in the *Slow Loop* (25 MHz) is realized as a seven states state-machine for hardware reuse and loop rate improvement. This results in an overall compensator loop rate of 2.78 MHz. The ADCs' analog anti-aliasing filters have a bandwidth of approximately 1 MHz and satisfy the Nyquist frequency of the loop rate. In this particular implementation a single demodulators D1 is realized. After each compensator and demodulator iteration the results are transferred back to the *Fast Loop*.

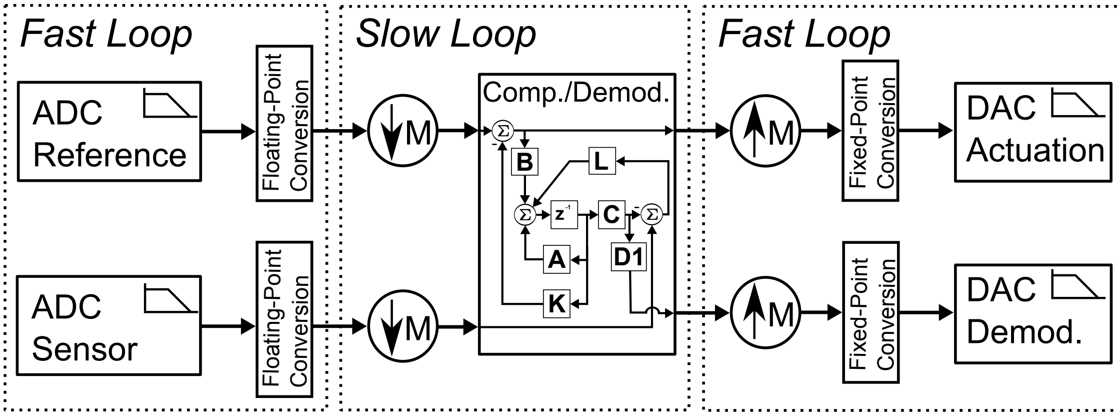


Figure 6: Overview of the full implementation in the nano analytik GmbH SPM platform.

## V. RESULTS AND DISCUSSION

The functionality of the extended compensator is investigated in the following, both in the time domain and during imaging. The adapted AFM setup utilized is shown in Figure 7, with the implementation of a single eigenmode compensator and demodulator. The Lock-in amplifier usually used is removed from the feedback loop. The AFM controller is switched to contact mode and the presented methodology is connected.

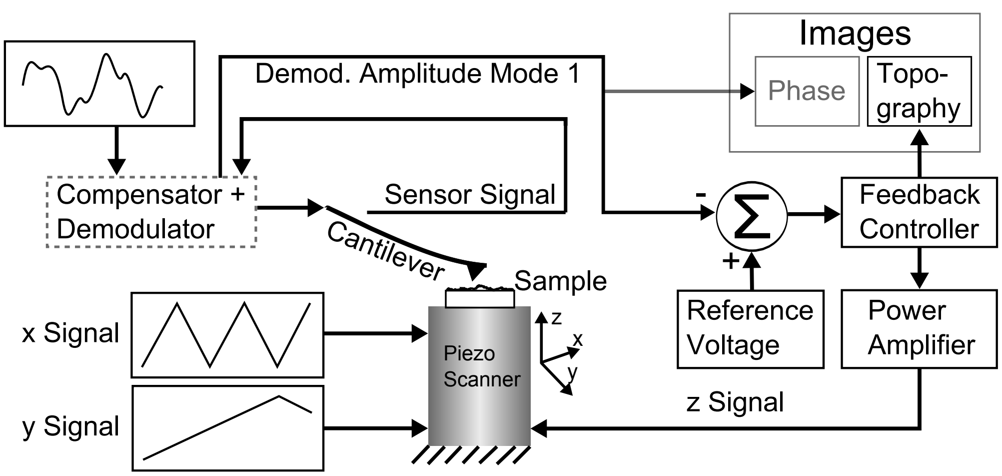


Figure 7: Modified setup with the compensator and demodulator shown in a dashed box, delivering the demodulated amplitude for the z feedback loop.

## A. Time Domain Results

The amplitude detector evaluated in the time domain is presented in Figure 8. The bottom graph in Figure 8(a) is an amplitude modulated test signal with a modulation depth of about 15 %. It forms the input to a standalone demodulator. The top curve in Figure 8(a) is the demodulated signal, representing the envelope of the bottom input signal. The clearly resolved amplitude shows intermediate steps upon a change in amplitude. As explained in Section 2, its nature lies in the evaluation of the amplitude every half period of a cantilever vibration cycle. The resulting demodulated signal is amplified and hence does not exactly match the numerical difference of the two input amplitudes.

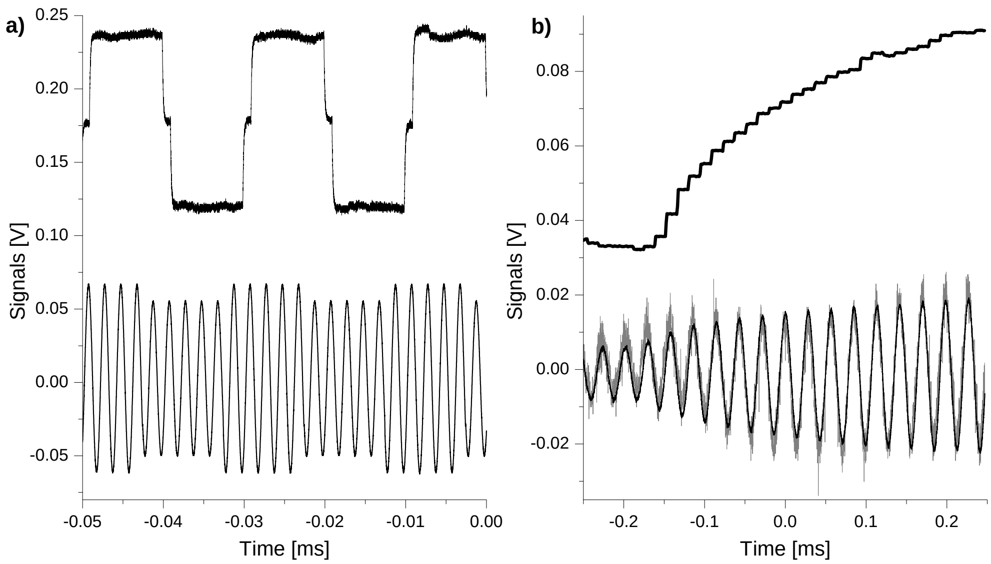


Figure 8: The bottom curves in both sub-figures show input data to the compensator/demodulator. The top curves indicate the demodulated amplitudes. a) is performed on a test signal using the demodulator only, b) is performed on a real active cantilever's deflection signal $y_k$ processed by the compensator and demodulator.

Figure 8(b) is the demodulation on a real active cantilever sensor signal. The noisy gray curve at the bottom of the diagram is the vibrating cantilever's deflection signal $y_k$ in the transition to a new amplitude. The black curve is the estimated $\hat{y}_{k,1}$. The top signal of Figure 8(b) is the demodulated amplitude as obtained by the implementation of Figure 6. The noise originally present in $y_k$ is reduced in its estimation $\hat{y}_{k,1}$. Hence, the demodulated amplitude is clearly resolved and usable for consecutive processing within the feedback loop.

## B. Imaging

The amplitude demodulation methodology presented is validated by imaging a calibration sample. Figure 9 is the image of a Nanodevices Inc. calibration grid with 200 nm deep line trenches and a 2 $\mu$m pitch. The set-point is 40 %, set as a corresponding static deflection in the contact mode AFM software. The imaging area is $(9\,\mu\text{m})^2$ at a rate of 2 lines/s. Additionally, the Q factor of the first resonance (76.249 kHz) is set to 100.

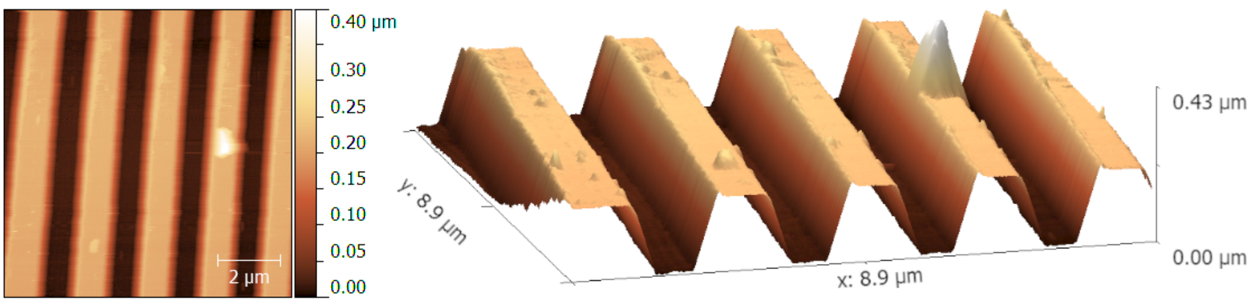


Figure 9: 2D and 3D view of an image of a calibration sample using the estimator based demodulator in the z feedback loop. The utilized cantilever resonance is the first transverse eigenmode with a modified Q factor of 100.

The time constant of the demodulation technique depends on the cantilever's time constant $\tau_1$. In this case, the Q factor of 100 results in $\tau_1 = 417\,\mu$s in free air. During imaging, the effective Q factor is considerably lowered at the set-point of 40 %, resulting in a smaller $\tau_1$. Following, the presented demodulation technique has its greatest benefits at low Q factors, such as during imaging in water. In that environment the presented technique can be helpful to increase the overall speed of the microscope.

# VI. CONCLUSION

Atomic force microscopy is a powerful but still relatively slow and complex instrument. The cantilever and demodulation techniques are two bottlenecks in the z feedback loop. Increasing the bandwidth of both components can potentially increase the imaging rates. Our previously developed compensator offers the potential to adjust the cantilever's Q factor and perform an amplitude demodulation simultaneously. The compensator delivers a filtered and decoupled cantilever deflection signal. The decoupling suppresses frequencies other than the frequencies of modeled eigenmodes, such as excited higher harmonics and noise. The amplitude demodulator is a simple extension to the compensator. It leads to a distortion free estimated amplitude that can be used in the z feedback loop. Given the estimator, the presented compensator/demodulation methodology is of lower overall complexity than attaching a compensator/Lock-in combination to the AFM. Decreased cantilever time constants, based on lower Q factors or higher resonance frequencies, can increase the demodulation speed and imaging bandwidth. The estimator based demodulator can be easily used for high speed imaging in higher eigenmodes. It can also be extended to work in a multi-eigenmode control approach for multifrequency AFM.

## VII. ACKNOWLEDGEMENTS

The research leading to these results has received funding from the European Union's Seventh Framework Programme FP7/2007-2013 under grant agreement no. 318804 (SNM) and ZIM-Project KF2114205NT2.

## REFERENCES

[1] G. Binnig, C. Quate, and C. Gerber, Physical Review Letters **56**, 930 (1986).
[2] M. L. Meade, Journal of Physics E: Scientific Instruments **15**, 395 (1982).
[3] T. Ando, N. Kodera, E. Takai, D. Maruyama, K. Saito, and A. Toda, Proceedings of the National Academy of Sciences of the United States of America **98**, 12468 (2001).
[4] F. Blais and M. Rioux, Signal Processing **11**, 145 (1986).
[5] J. Kokavecz, Z. Tóth, Z. L. Horváth, P. Heszler, and A. Mechler, Nanotechnology **17**, S173 (2006).
[6] K. S. Karvinen and Moheimani, S O R, The Review of scientific instruments **85**, 023707 (2014).
[7] R. Garcia and E. T. Herruzo, Nat Nano **7**, 217 (2012).
[8] N. F. Martinez, J. R. Lozano, E. T. Herruzo, F. Garcia, C. Richter, T. Sulzbach, and R. Garcia, Nanotechnology **19**, 384011 (2008).
[9] R. Proksch, Applied Physics Letters **89**, 113121 (2006).
[10] T. Ivanov, T. Gotszalk, T. Sulzbach, and I. W. Rangelow, Ultramicroscopy **97**, 377 (2003).

[11] M. Kaestner, T. Ivanov, A. Schuh, A. Ahmad, T. Angelov, Y. Krivoshapkina, M. Budden, M. Hofer, S. Lenk, J.-P. Zoellner, I. W. Rangelow, A. Reum, E. Guliyev, M. Holz, and N. Nikolov, Journal of Vacuum Science & Technology B, Nanotechnology and Microelectronics: Materials, Processing, Measurement, and Phenomena **32**, 06F101 (2014).

[12] I. W. Rangelow, S. Skocki, and P. Dumania, Microelectronic Engineering **23**, 365 (1994).

[13] Y. Kanda, IEEE Transactions on Electron Devices **29**, 64 (1982).

[14] A. A. Barlian, W.-T. Park, J. R. Mallon, A. J. Rastegar, and B. L. Pruitt, Proceedings of the IEEE. Institute of Electrical and Electronics Engineers **97**, 513 (2009).

[15] I. W. Rangelow, Microelectronic Engineering **83**, 1449 (2006).

[16] I. W. Rangelow, Journal of Vacuum Science & Technology A: Vacuum, Surfaces, and Films **21**, 1550 (2003).

[17] G. Jóźwiak, D. Kopiec, P. Zawierucha, T. Gotszalk, P. Janus, P. Grabiec, and I. W. Rangelow, Sensors and Actuators B: Chemical **170**, 201 (2012).

[18] T. Michels, E. Guliyev, M. Klukowski, and I. W. Rangelow, Microelectronic Engineering **97**, 265 (2012).

[19] nano analytik GmbH, (http://www.nanoanalytik.net/).